# The Dynamics of Multiple Neck Formation and Fragmentation in High Rate Extension of Ductile Materials

P.R. Guduru and L.B. Freund
Division of Engineering, Brown University, Providence, RI 02912

**ABSTRACT**
Dynamic necking bifurcation in rapidly extending cylindrical rods is investigated. It has been found that both short wavelength and long wavelength perturbations are suppressed by inertia and an intermediate wavelength is favored. The analysis predicts an increase in the number of necks and an increase in the bifurcation strain with increasing extension rate, in agreement with the experimental observations. In terms of the number of necks formed as a function of extension rate, good agreement has been found between the experiments and the analysis. At any given aspect ratio, the model also predicts that the number of necks increases rapidly beyond a critical extension rate. Currently no experimental results are available to verify this prediction.

**KEYWORDS**
Necking bifurcation, ductility, fragmentation, plasticity.

## INTRODUCTION

The necking instability in rods under quasi-static uniaxial loading has been studied by Miles[1], Cheng et al. [2], Hutchinson & Miles [3] and Hill & Hutchinson [4]. The general approach has been to use perturbation analysis in order to determine the critical stress state at which a non-homogeneous, neck-like deformation field can exist. Hutchinson and Miles [3] showed that such a deformation field can exist at a critical stress, which is greater than the stress at maximum load, and the lowest critical stress corresponds to the longest wavelength perturbation, in other words, a single neck is formed at this critical stress. However, fragmentation experiments of Grady & Benson [5] and Altynova *et al*. [6] have demonstrated that rapidly expanding rings form multiple necks and some of these necks fail, leading to fragmentation of the rings. Shenoy and Freund [7] generalized the perturbation analysis of Hill and Hutchinson [4] to study a rectangular block of material, dynamically loaded in plane strain, using a hypoelastic constitutive relation. They examined the growth rate of neck-like perturbations and found that short as well as long wavelength perturbations are suppressed and intermediate wavelengths have the highest rate of growth. Their analysis captured the qualitative features of the experimental observations such as the increasing number of necks and the increasing ductility with an increase in extension rate. However, direct comparison with experiments could not be performed as it was a plane strain analysis. In this paper, the perturbation analysis of Shenoy and Freund [7] is adapted to an extending cylinder in order to facilitate comparison with experiments. This work is a generalization of the analysis of Hutchinson and Miles [3] to include inertial effects. The next section discusses the homogeneous solution to the extending rod problem, followed by a section on perturbation analysis. Results and a brief discussion are presented at the end.

### HOMOGENEOUS DEFORMATION

Consider an incompressible cylindrical rod of radius A and length 2L, undergoing homogeneous deformation in the axial direction, as shown in Fig. 1. The ends of the rod move with a speed $v_0$ as shown. Denoting the reference coordinates as (R, Θ, Z) and current coordinates as (r, θ, z), the deformation is described as

$$r = \lambda^{-1/2} R, \qquad z = \lambda Z \tag{1,2}$$

where

$$\lambda = 1 + v_0 t / L \tag{3}$$

with $t$ representing time. Using eq. (1)-(3), the velocity field corresponding to the homogeneous deformation state is

$$v_r = -\frac{v_0}{2L} R\left(1+\frac{v_0}{L}t\right)^{-3/2}, \qquad v_z = \frac{v_0}{L} Z \tag{4,5}$$

The fields $v_r(R,Z,t)$ and $v_z(R,Z,t)$ are the radial and axial components of velocity. The Cauchy stress ($\boldsymbol{\sigma}$) for this homogeneous 1-D deformation is

$$\boldsymbol{\sigma} = \begin{pmatrix} 0 & 0 & 0 \\ 0 & 0 & 0 \\ 0 & 0 & \sigma \end{pmatrix} + \begin{pmatrix} -p & 0 & 0 \\ 0 & -p & 0 \\ 0 & 0 & -p \end{pmatrix} \tag{6}$$

where $\sigma$ is the axial stress due to strain history and $p$ is the hydrostatic stress due to particle acceleration ( see eq.(4)). Using the equation of motion in the radial direction and the condition that $p$=0 at $R$=$A$, $p$ can be determined to be [7]

$$p = \frac{3}{8}\rho\left(\frac{v_0}{L}\right)^2 \frac{(A^2-R^2)}{(1+v_0 t/L)^3} \tag{7}$$

In the above equation, $\rho$ is the mass density. Eq. (4) and (5) describe the deformation state and $\sigma$ is not known since no constitutive relation has been used yet. The stability of this deformation state is analysed next. In other words, if the velocity field given by eq. (4) and (5) is slightly perturbed in a way that is consistent with the boundary conditions, we examine if such a perturbation grows in time and, if it does, what is its rate of growth.

## LINEAR PERTURBATION ANALYSIS

The equations of motion in the rate form in terms of the components of the first Piola Kirchoff stress $\boldsymbol{T}$ are

$$\dot{T}_{Rr,R} + \dot{T}_{Zr,Z} + (\dot{T}_{Rr} - \dot{T}_{\Theta\theta})/R = \rho\ddot{v}_r \tag{8}$$

$$\dot{T}_{Rz,R} + \dot{T}_{Zz,Z} + \dot{T}_{Rz}/R = \rho\ddot{v}_z \tag{9}$$

All derivatives with respect to Θ are set to zero in writing these equations. The boundary conditions are

$$v_z(R,\pm L,t) = \pm v_0, \qquad \dot{T}_{Zr}(R,\pm L,t) = 0 \tag{10,11}$$

$$\dot{T}_{Rz}(A,Z,t) = 0, \qquad \dot{T}_{Rr}(A,Z,t) = 0 \tag{12,13}$$

In the above equations, $\dot{\boldsymbol{T}}$ can be expressed in terms of the current stress and deformation quantities using

$$\dot{\boldsymbol{T}} = \boldsymbol{F}^{-1}(\hat{\boldsymbol{\sigma}} - \boldsymbol{D}\boldsymbol{\sigma} - \boldsymbol{\sigma}\boldsymbol{W}) \tag{14}$$

where $\boldsymbol{F}$ is the deformation gradient, $\hat{\boldsymbol{\sigma}}$ is the Jaumann rate of Cauchy stress, $\boldsymbol{D}$ and $\boldsymbol{W}$ are the symmetric and antisymmetric parts of the velocity gradient. The material is assumed to follow the hypoelastic constitutive relation developed by Storen and Rice [8], which in the present context becomes

$$\hat{\sigma}'_{rr} = (h+h_1)D_{rr} + (h-h_1)D_{\theta\theta} \tag{15}$$

$$\hat{\sigma}'_{\theta\theta} = (h-h_1)D_{rr} + (h+h_1)D_{\theta\theta} \tag{16}$$

$$\hat{\sigma}'_{zz} = 2hD_{zz} \tag{17}$$

$$\hat{\sigma}'_{rz} = 2h_1 D_{rz} \tag{18}$$

where prime denotes the deviatoric component. In writing eq. (15)-(18), it was assumed that $v_\theta$ = 0, all derivatives with respect to $\theta$ are zero and $D_{rr} + D_{\theta\theta} + D_{zz} = 0$. Here $h$ and $h_1$ are the tangent modulus and the secant modulus of the graph of equivalent stress $\sqrt{\sigma'_{ij}\sigma'_{ij}/2}$ vs. equivalent strain $\sqrt{2\varepsilon_{ij}\varepsilon_{ij}}$. This curve reduces to the shear stress – shear strain curve in pure shear. It can be verified that the homogeneous solution given by eq. (4)-(7) satisfies eq. (8)-(18). In addition, $\sigma$ at any time can be calculated by integrating eq. (15)-(18).

Introduce, at some time τ, a perturbation velocity field $(v_r', v_\theta', v_z')$ such that $v_\theta'=0$, and $v_r'$ and $v_z'$ do not depend on $\theta$. Then, it can be seen that this perturbation velocity field, along with the corresponding perturbation stress field satisfies eq. (8)-(18), with eq.(10) modified as

$$v_z'(R,\pm L,t)=0 \tag{19}$$

Dropping the prime for convenience, eq.(8)-(9) and eq. (11)-(19) are the governing equations for the perturbation velocity field and the task is now reduced to analyzing the evolution of this field. Without loss of generality, τ can be set to zero, so that $\boldsymbol{F}=\mathbf{1}$ and the reference and current configurations coincide with each other. Note that eq. (15)-(18) do not determine the hydrostatic component of the stress rate and, in order to eliminate it, eq. (8) is differentiated with respect to $z$ and eq. (9) with respect to $r$ and subtracted from one another. This results in

$$\left(\dot{T}_{rr}-\dot{T}_{zz}\right)_{,zr}+\dot{T}_{zr,zz}+\left(\dot{T}_{rr}-\dot{T}_{\theta\theta}\right)_{,z}/r-\dot{T}_{rz,rr}-\dot{T}_{rz,r}/r+\dot{T}_{rz}/r^2=\rho\left(\ddot{v}_{r,z}-\ddot{v}_{z,r}\right) \tag{20}$$

Since the material is incompressible, $v_r$ and $v_z$ can be written in terms of a potential $\varphi(r,z,t)$ as $v_r=-\varphi_{,z}$ and $v_z=\frac{1}{r}(r\varphi)_{,r}$. Defining $\alpha=\frac{3}{4}\rho\left(v_0/L\right)^2$ and using eq. (14)-(18), eq. (20) becomes

$$\frac{1}{2}(\sigma-2h_1)\varphi_{,rrrr}-\frac{1}{2}(\sigma+2h_1)\varphi_{,zzzz}-(3h-h_1)\varphi_{,rrzz}+\frac{1}{r}(\sigma-2h_1)\varphi_{,rrr}-\frac{1}{r}(3h-h_1)\varphi_{,rzz}-$$
$$\frac{3}{2r^2}(\sigma-2h_1)\varphi_{,rr}+\left(\frac{3h-h_1}{r^2}-\alpha\right)\varphi_{,zz}+\frac{3}{2r^3}(\sigma-2h_1)\varphi_{,r}-\frac{3}{2r^4}(\sigma-2h_1)\varphi=$$
$$\rho\left(-\ddot{\varphi}_{,rr}-\ddot{\varphi}_{,zz}-\frac{\ddot{\varphi}_{,r}}{r}+\frac{\ddot{\varphi}}{r^2}\right) \tag{21}$$

Assuming a separable solution of the form

$$\varphi(r,z,t)=\psi(r,z)T(t) \tag{22}$$

results in an equation for $\psi(r,z)$ as

$$\frac{1}{2}(\sigma-2h_1)\psi_{,rrrr}-\frac{1}{2}(\sigma+2h_1)\psi_{,zzzz}-(3h-h_1)\psi_{,rrzz}+\frac{1}{r}(\sigma-2h_1)\psi_{,rrr}-\frac{1}{r}(3h-h_1)\psi_{,rzz}+$$
$$\left(\rho\theta^2-\frac{3}{2r^2}(\sigma-2h_1)\right)\psi_{,rr}+\left(\frac{3h-h_1}{r^2}+\rho\theta^2-\alpha\right)\psi_{,zz}+\left(\frac{3}{2r^3}(\sigma-2h_1)+\rho\theta^2/r\right)\psi_{,r}-$$
$$\left(\frac{3}{2r^4}(\sigma-2h_1)+\rho\theta^2/r^2\right)\psi=0 \tag{23}$$

where $\theta^2=\frac{\ddot{T}}{T}$, is the separation constant. If $\theta^2$ is real and positive, the perturbation field is unstable. Assume a separable solution once again.

$$\psi(r,z)=g(r)\cos(\gamma z) \tag{24}$$

In order to satify the boundary condition eq.(19),

$$\gamma=\frac{\pi q}{2L},\quad q=1,3,5,\ \ldots \tag{25}$$

Using eq.(24) in eq. (23), the governing equation for $g(r)$ is obtained as

$$g''''+\frac{2}{r}g'''+\left(\frac{\gamma^2(3h-h_1)+\rho\theta^2}{\sigma/2-h_1}-\frac{3}{r^2}\right)g''+\left(\frac{\gamma^2(3h-h_1)+\rho\theta^2}{r(\sigma/2-h_1)}+\frac{3}{r^3}\right)g'-$$
$$\left(\frac{\gamma^2(3h-h_1)+\rho\theta^2}{r^2(\sigma/2-h_1)}+\frac{3}{r^4}+\frac{\gamma^2\left(\rho\theta^2-\alpha\right)+\gamma^4(\sigma/2+h_1)}{\sigma/2-h_1}\right)g=0 \tag{26}$$

Assuming a power law type uniaxial stress-strain relation,

$$\sigma=k\varepsilon^n \tag{27}$$

where $k$ and $n$ are material constants, $n$ denoting the strain hardening exponent. Also, $n=h/h_1$. By defining

$$b=[3-1/n+12N(v_0/v_p)^2/(\pi^2q^2n(ns)^{n-1})]/(3s-2/n)$$
$$c=[(1/n+3s/2)+3(4N-3)(v_0/v_p)^2/(\pi^2q^2n(ns)^{n-1})]/(1/n-3s/2)$$

in which $s = \sigma / 3h$, $v_p = \sqrt{k/\rho}$ and $N = \left(L\theta / v_0\right)^2$, eq.(26) can be written as

$$\boldsymbol{L}^2(g) + 2b\gamma^2\,\boldsymbol{L}(g) + c\gamma^4 g = 0 \tag{28}$$

where the operator $\boldsymbol{L}$ is defined by $\boldsymbol{L}(g) = g'' + g'/r - g/r^2$. Further, by setting ${\rho_1}^2 = b - \sqrt{b^2 - c}$ and ${\rho_1}^2 = b + \sqrt{b^2 - c}$, eq.(28) can be represented as

$$\left(\boldsymbol{L} + \gamma^2{\rho_1}^2\right)\left(\boldsymbol{L} + \gamma^2{\rho_2}^2\right)g = 0 \tag{29}$$

The boundary conditions eq. (12) and (13) give

$$g''(A) + \frac{1}{A}g'(A) + \left(\gamma^2 - 1/A^2\right)g(A) = 0 \tag{30}$$

$$g'''(A) + \frac{2}{A}g''(A) + \left(2b\gamma^2 - 1/A^2\right)g'(A) + \left\{\frac{1}{A^3} + \frac{2\gamma^2}{A}\left(b - \frac{h_1}{\sigma/2 - h_1}\right) + \frac{\gamma^2\alpha A}{\sigma/2 - h_1}\right\}g(A) = 0 \tag{31}$$

Nontrivial solutions of eq. (29) are sought subject to constraints eq.(30) and (31). The solution to eq.(29) has different forms depending on the complex character of ${\rho_1}^2$ and ${\rho_2}^2$. The relevant case here is the one when ${\rho_1}^2$ and ${\rho_2}^2$ form a complex conjugate pair, in which case eq.(29) admits a solution of the form

$$g(r) = BJ_1(\gamma\rho r) + \overline{B}\,J_1(\gamma\,\overline{\rho} r) \tag{32}$$

where bar denotes complex conjugate, $B$ is an arbitrary complex constant, $\rho$ a square root of either ${\rho_1}^2$ or ${\rho_2}^2$ and $J_n$ is the Bessel function of order $n$. Subject to eq. (30) & (31), the condition for the existence of a non-trivial $B$ is

$$\boldsymbol{Im}\left\{\left(1 - \overline{\rho}^2\right)J_1\left(\gamma\overline{\rho}A\right)\left[\left(C_1 - C_2\right)J_1\left(\gamma\rho A\right) + \gamma\rho A\left(C_3 - \rho^2\right)J_0\left(\gamma\rho A\right)\right]\right\} = 0 \tag{33}$$

where

$$C_1 = \frac{\frac{9}{4}\left(A/L\right)^2\left(v_0/v_p\right)^2}{n(ns)^{n-1}\left(3s/2 - 1/n\right)},\; C_2 = \frac{2}{\left(3ns/2 - 1\right)} \text{ and } C_3 = \frac{3\left(1 - s/2\right)}{\left(3s/2 - 1/n\right)} + \frac{12N\left(v_0/v_p\right)^2}{\pi^2 q^2 n(ns)^{n-1}\left(3s/2 - 1/n\right)}$$

In the above equations, $N$ represents the rate of growth of the perturbation relative to the background homogeneous rate of stretch. $N$ is required to be large compared to 1 for a perturbation mode $q$ to result in multiple necking. For a given strain hardening exponent $n$, stress $s$, aspect ratio $A/L$, extension speed $v_0/v_p$ and perturbation mode $q$, eq.(33) determines the rate of growth $N$.

## RESULTS AND DISCUSSION

The calculation procedure is described first. For a given $n$, aspect ratio $\beta = A/L$, stress $s$ and extension rate $v_0/v_p$, eq. (33) is solved for $N$ as a function of $q$. The value of $q$ corresponding to the maximum value of $N$ ($N_{max}$) is termed $q_{max}$ and it represents the dominant perturbation mode for these conditions. However, we require $N_{max} >> 1$ for this perturbation mode to turn in to a necking mode. Hence, a given mode $q_{max}$ is supposed to satisfy a failure criterion when $N_{max} = N_C$, where $N_C$ is an arbitrarily chosen large number. In the following analysis, $N_C$ is chosen to be 200. If $N_{max} < N_C$, $s$ is increased gradually until $N_{max} = N_C$. The corresponding $s$ is the critical stress ($s_c$) for necking bifurcation. The fragmentation experiments of Grady & Benson [5] and Altynova *et al.* [6] show the following qualitative features. (i) The number of necks/fragments increases with an increase in extension rate. (ii) The fracture strain increases with an increase in extension rate. The current analysis quantifies these observations, as illustrated in Fig. 2 and Fig. 3. Fig. 2 shows the number of necks as a function of extension rate, for different hardening exponents. The analysis predicts that the hardening exponent has little effect on the number of necks, within the range of $v_0/v_p$ plotted in Fig. 2. Fig. 3 shows an almost linear increase in critical strain, which is again independent of the hardening exponent. One of the drawbacks of the analysis presented above is the arbitrary choice of $N_C$. However, the number of necks is weakly dependent on $N_C$. An increase in $N_C$ from 100 to 2000 results in an increase in the number of necks by a factor of 2-3. Thus, a judicious choice of $N_C$ could possibly be made from an appropriate comparison with experiments. Comparison

of the perturbation analysis results with those of the experiments requires information about the constitutive behavior of the material at the high strain rates. Typical strain rate in the experiments of Grady and Benson [5] on aluminum and copper rings was around $10^4$/s. For these materials, this is also the strain rate around which there is a sharp increase in the flow stress. Thus, the accuracy of the constitutive data available places a limitation on the comparison with the experimental results. Fig. 4 compares the number of necks observed in the fragmentation experiments of Grady & Benson [5] on OFHC copper rings with the model predictions, for four different choices of $N_C$. Constitutive parameters used are $k=760MPa$ and $n=0.49$ (strain rate 1.2 x $10^4$ /s, Follansbee [9]). A value of 125-200 for $N_C$ appears to fit the experiments well. Similar comparison for 1100-O aluminum is shown in Fig.5. Constitutive parameters used are, $k=230MPa$ and $n=0.33$ (strain rate $10^3$ /s, Pao & Gilat [10]). A choice of 150-250 for $N_C$ appears to yield god agreement. Figs. 6 and 7 show the comparison between the bifurcation strain from the analysis and the fracture strain measured by Grady and Benson [5] for the same materials. Fracture strain, defined as the change in the total length of all fragments with respect to the initial ring length, always overestimates the bifurcation strain. In spite of that, the model captures the magnitude and the trend of fracture strain quite well. Fig. 8 shows the variation of the number of necks over a larger range of extension rate, for several aspect ratios. The number of necks is seen to increase rapidly beyond a critical extension rate and this rate decreases as the aspect ratio increases. As the number of necks increases rapidly, the stress is seen to saturate at the same value for all aspect ratios and this level is found to be a decreasing function of the hardening exponent. However, no experimental results are currently available to test the validity of this prediction.

## CONCLUSIONS

A linear perturbation analysis of extending cylindrical rods has been carried out and it captures all the qualitative features of the fragmentation experiments, such as the increase in the number of fragments and fracture strain with increase in extension speed. Good quantitative agreement between the model predictions and the experimental results has been found for a choice of $N_C$ in the range of 100-250. Moreover, the choice of the range of $N_C$ that yields good agreement with experiments for two different materials is almost the same. This implies a predictive capability for the current analysis. The constitutive law for the materials used in the experiments is very rate sensitive at the strain rates encountered during rapid extension. Thus, the accuracy of constitutive data is an important ingredient in using the perturbation analysis. The model also makes other predictions on the effect of aspect ratio on the number of necks and fracture strain and the effect of the extension speed on the number of necks beyond a critical speed. More detailed experimental results are necessary to test these predictions.

**Acknowledgements**
The research support of the Office of Naval Research grant N00014-95-1-0239 and the Department of Energy, Office of Basic Engineering Sciences grant DE-FG02-95-ER14561 is gratefully acknowledged.

**References**

[1] Miles J.P. (1970). *J. Mech. Phys. Solids*. 19, 89-102.
[2] Cheng S.Y., Ariaratnam S.T. and Dubey R.N. (1971). *Quart. Appl. Math* 29, 41-51.
[3] Hutchinson J.W. and Miles J.P. (1974). *J. Mech. Phys. Solids*. 22, 61-71.
[4] Hill R. and Hutchinson J.W. (1975) *J. Mech. Phys. Solids*. 23, 239-264.
[5] Grady D.E. and Benson D.A. (1983) *Exper. Mech*. 12, 393-400.
[6] Altynova M., Hu X. and Daehn G.S. (1996) *Metall. Mater. Trans*. 27A, 1837-1844.
[7] Shenoy V.B. and Freund L.B. (1999) *J. Mech. Phys. Solids*. 47, 2209-2233.
[8] Storen S and Rice J.R.(1975) *J. Mech. Phys. Solids*. 23, 421-441.
[9] Follansbee, P.S. (1986) In *Metallurgical Applications of Shock-wave and high-strain-rate phenomena*, ed. Murr, L.E., Staudhammer, K.P. and Meyers, M.A., p. 451.
[10] Pao Y.H. and Gilat A. (1989) *Int. J. Plasticity*. 5, 183-196.

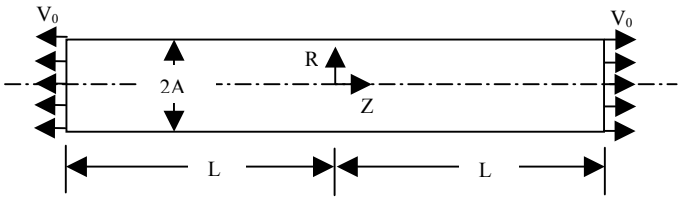


Figure 1. Geometry of the deforming cylinder

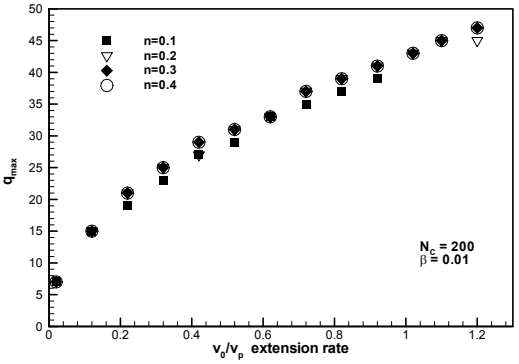


Figure 2. Number of necks as a function of extension rate.

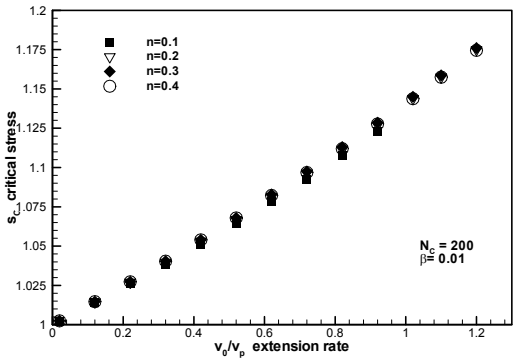


Figure 3. Variation of critical stress with extension rate

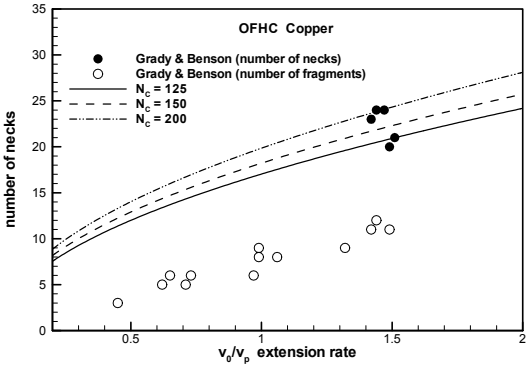


Figure 4. Comparison with experiments for OFHC copper

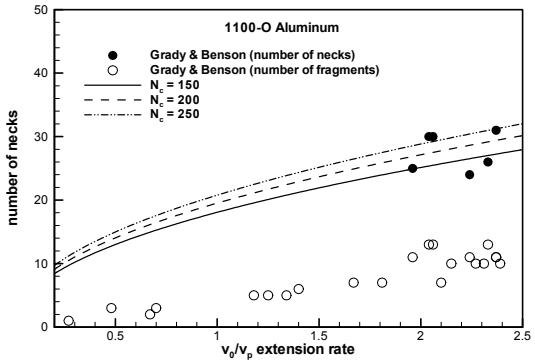


Figure 5. Comparison with experiments for 1100-O aluminum

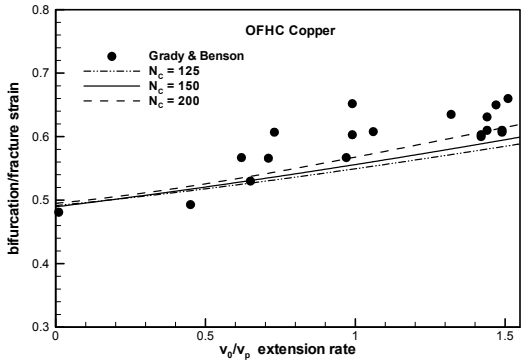


Figure 6. Fracture strain comparison for OFHC copper

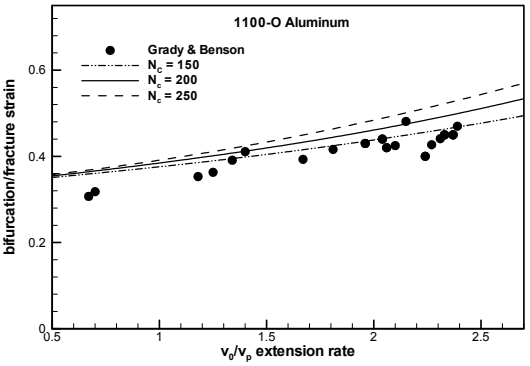


Figure 7. Fracture strain comparison for 1100-O aluminum

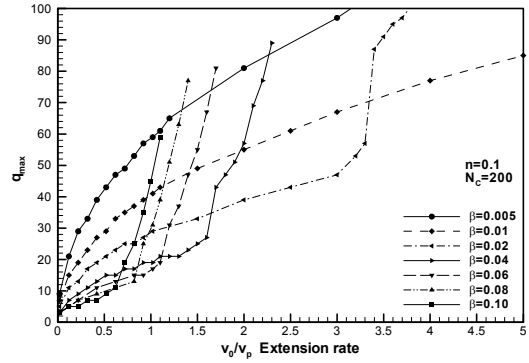


Figure 8. Variation of number of necks at high extension rates